Graphene oxide-templating of superconducting $YBa_2Cu_3O_{7-\partial}$

Rebecca Boston‡, O. Alexander Bell‡, Valeska P. Ting, Andrew T. Rhead, Tadachika Nakayama, Charl F. J. Faul and Simon R. Hall*

R Boston[†], Bristol Centre for Functional Nanomaterials, University of Bristol, Bristol, BS8 1FD, UK

R. Boston, O. A. Bell, C. F. J. Faul and S. R. Hall, School of Chemistry, University of Bristol, Bristol, BS8 1TS

V. P. Ting, Department of Chemical Engineering, University of Bath, Bath, BA2 7AY

A. T. Rhead, Department of Mechanical Engineering, University of Bath, Bath, BA2 7AY

T. Nakayama, Department of Electrical Engineering, Nagaoka University of Technology, 1603 1 Kamitomioka, Nagaoka, Niigata, 940 2188, Japan

Graphene oxide, templating, functional oxides, superconductors

ABSTRACT: We report the first use of a graphene oxide (GO) template for synthesis of the complex functional material yttrium barium copper oxide (YBCO), producing well-defined YBCO structures that replicate the micro- and macromorphology of the GO template. Two morphologies (foam and layered paper-like) are demonstrated to show the utility of GO as a template. The templated YBCO materials are found to be almost phase-pure in the superconducting $YBa_2Cu_3O_{7-\delta}$ (Y123) form. The mechanism of GO-templating is elucidated, and superconductive properties exceeding those of materials produced by typical high-temperature solid-state syntheses are found for the templated materials.

The templated synthesis of inorganic materials is an actively researched field,[1,2] with materials for applications such as piezoelectrics,[3] solid oxide fuel cells[4] and catalysts[5] all being created using this flexible and wide-ranging technique. The use of biologically-derived templates has yielded a number of hitherto unavailable morphologies in complex oxide materials, such as nanowires,[6,7] microspheres,[8] and more complex structures.[9] Template-based synthesis pathways have also given greater insight into the fundamental mechanisms that govern nanoscale crystal growth.[10] Typically highly carbonaceous and strongly chelating, these templates prevent agglomeration and sintering of stable intermediates during high temperature syntheses. This allows the formation of the desired phase without slow and energy-intensive heating and grinding steps[11] thus templated syntheses are more efficient, whilst still allowing for fine control of phase and morphology.

Whilst nano- and micrometer-scale growth of crystallites using biotemplates is well understood, it is challenging to up-scale this control to create well-ordered macroscopic structures. This is possible by use of a sacrificial template, which directs the morphology at the chosen length scale[12,13] and is destroyed during synthesis, leaving the final inorganic product as a polycrystalline replica.[14,15] This allows, for example, construction of monolithic inverse opaline crystals from simple oxides such as SiO_2 and TiO_2[16] or metals.[17] There are many prior examples of simple oxides constructed from sacrificial templates, but their use for ternary or quaternary materials, such as complex metal oxides like $YBa_2Cu_3O_{7-\delta}$ (Y123), remains relatively rare.[18–21] Y123 is an excellent model system for testing the efficacy of templating methods in complex oxides due to the strong dependence of the superconducting properties of Y123 upon the templated morphology and phase purity.

Graphene oxide (GO) is a promising material for templating metal oxides, showing effective templating of SiO_2 into a nanoflake morphology.[22] GO consists of single-atom-thick carbon sheets, but differs markedly from graphene. GO contains a random oxygen-rich network of sp^3-hybridised carbon atoms, interspersed with islands of pristine sp^2-hybridised graphitic carbon[23,24] (from which GO is initially synthesized). GO is capable of uptake of transition metal ions (for example Cu^{2+}) from solution[25] as well as forming three-dimensional macroporous solids,[26,27] hydrogels,[28] and papers[29] from aqueous dispersions. The wide variety of available final morphologies from a single material,[30] combined with an abundance of chelating hydroxyl and ketone functionalities,[24,31] makes GO attractive for use as a template for oxide materials.

Here we present the first instance of GO-templating of a quaternary metal oxide and demonstrate the use of monolithic GO porous templates to produce superconducting Y123. Two morphologies of GO (foam and paper) were chosen; both were synthesized from GO aqueous solutions by previously reported methods[26,29] and were successfully used to obtain superconducting Y123 structures with highly porous, or oriented structures, respectively. The resulting Y123 materials demonstrate an improvement in critical current density of the superconducting phase when compared with solid-state synthesis.[32,33]

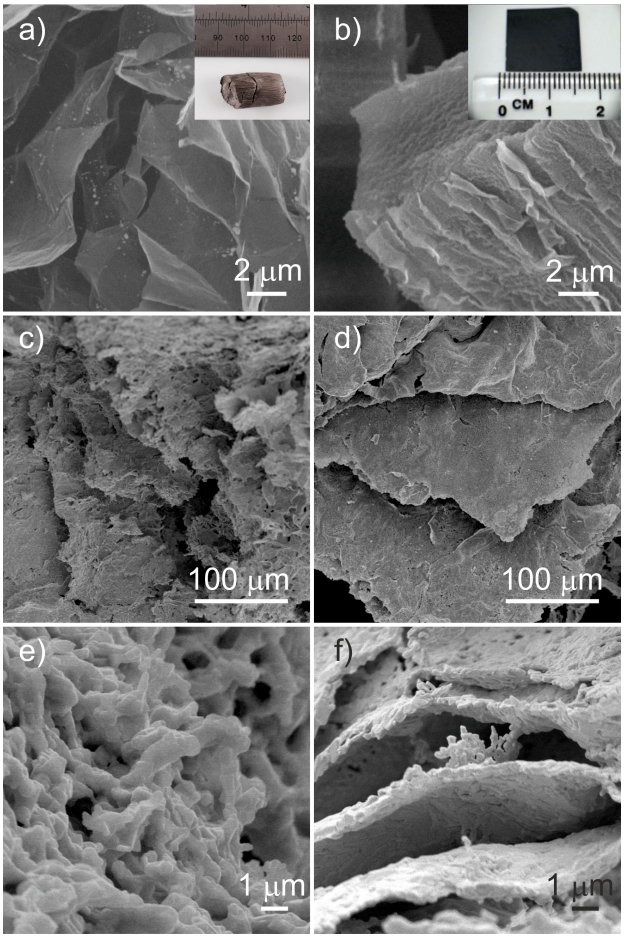

Figure 1. SEM micrographs of a) foam and b) paper templates prior to combination with the precursor solution, with inset photographs of each. c) and d) show micrographs of the calcined Y123 foam and layered structure respectively, with the microstructures shown in e) and f).

Full details of the experimental methods can be found in the supporting information, but briefly, monolithic GO structures with foam and layered paper-like microstructure were immersed in aqueous solutions of Y, Ba, and Cu nitrate salts. Soaked templates were then dried and calcined to obtain templated YBCO. Initially the structure of the template and inorganic replicas were investigated using SEM, as shown in Figure 1. Figure 1a and Figure 1b show SEM micrographs of the GO foam and paper respectively, prior to soaking in the precursor, with inset photographs showing the macroscopic monoliths. SEM micrographs of the two templated solid structures (Figure 1c-f) show retention of the templates' porous (foam) and highly layered (paper) structures, respectively. The templated products show a polycrystalline structure, arranged in the same morphology and microstructure as the GO templates.

Non-destructive imaging by X-ray micro-computed tomography (X-ray μ-CT) revealed an interconnected macroporous internal structure (Figure 2). Figure 2a shows a model of the macropores present within a small section of the Y123 foam, with Figure 2b showing a cut-away of the sample illustrating the micron-scale porous internal stucture. This structure is a good replica of the

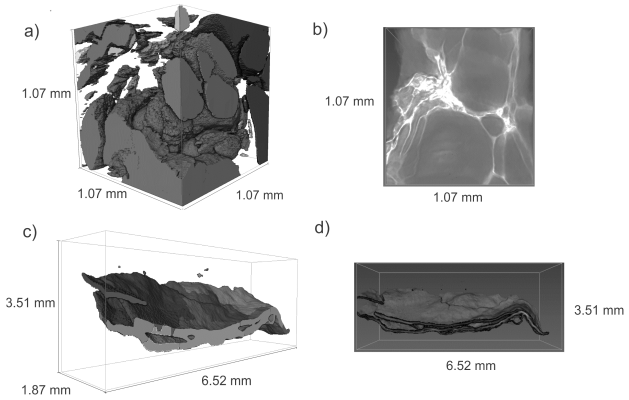

Figure 2. X-ray μ-CT images of a) and b) the Y123 foam showing, respectively, internal macro-pore structure and solid pore walls, and c) and d) the Y123 paper showing, respectively, internal layered structure and detailed morphology.

GO template, and indicates that the porous structure is retained throughout the sample during calcination.The pore mapping was used to obtain an average porosity of 42%. The structure of the paper-like Y123 is displayed in Figure 2c, with Figure 2d showing the layered structure is present throughout the sample, imparted by the GO template.

The composition of both the foam- and paper-templated Y123 was determined using TEM/EDX (Figure S1) and powder X-ray diffraction (Figure S2). The majority phase in both the foam and paper materials (Figure S2a and Figure S2b respectively) is $YBa_2Cu_3O_{6.9}$ (JCPDS card 79-0653), which is consistent with optimal oxygenation. A small number of impurity phases were also observed, including CuO, $BaCuO_2$ and Y_2BaCuO_5.

The mechanism by which this novel template acts to produce Y123 was investigated with a series of increasing calcination temperatures. Figure 3 shows the indexed PXRD patterns of samples heated to temperatures between 200 °C and 900 °C (at 100 °C intervals) and suggests that this synthesis proceeds *via* a different low-temperature pathway to that which has been observed previously with some polysaccharide biotemplates.[10–12] The synthesis does, however, show some similarities to the high carbon-content dextran-based syntheses,[8] as might be expected given the high carbon content of GO.

At 200 °C, the major crystalline phases present are the precursor materials barium and copper nitrates (JCPDS cards 76-1376 and 45-0594 respectively). As fully chelated ions are non-crystalline and therefore do not appear in the XRD pattern, the presence of these crystalline phases at these low temperatures is due to recrystallization of excess precursor solution present on the surface of the template upon drying. Barium nitrate is observed in greater quantities than the other two ions due to the fact that yttrium nitrate thermally decomposes below 200 °C, and copper nitrate between 200 °C and

300 °C (accounting for the small quantities observed at these temperatures).

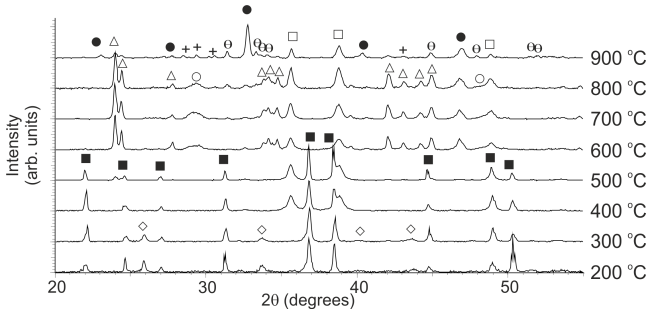

Figure 3. Temperature study of the formation of the Y123 phase. Phases present are $Ba(NO_3)_2$ (■), $Cu(NO_3)_2(H_2O)_3$ (◊), $YBa_2Cu_3O_{6.9}$ (⍰), CuO (□), $BaCO_3$ (Δ), Y_2O_3 (O), $BaCuO_2$ (+) and $Y_2Cu_2O_5$ (θ).

Between 300 °C and 400 °C the copper ions chelated in the monolith react with the template to form copper(II) oxide (JCPDS card 74-1021) which, crucially, allows for the retention of the template structure while the desired inorganic phase forms. Between 400 °C and 600 °C, as the template fully decomposes, the Ba^{2+} and Y^{3+} ions react to form yttrium oxide and barium carbonate (JCPDS cards 74-1828 and 41-0373 respectively), which are homogeneously spread throughout the material.

The next significant change in the sample occurs in the 800 °C and 900 °C interval, where a solid-solid reaction between Y^{3+}, Ba^{2+} and Cu^{2+} ions occurs due to the decomposition of $BaCO_3$ above 811 °C. In this templated approach, however, the time over which this reaction occurs is reduced to two hours due to the higher degree of mixing between the three precursor ions provided by the chelating template. The synthesis then proceeds as observed previously in typical biotemplated systems,[8,34] with Y123 emerging as the major phase between 800 °C and the final calcination temperature, 920 °C. Small quantities of $Y_2Cu_2O_5$ (JCPDS card 33-0511) and $BaCuO_2$ (JCPDS card 70-0441) are also observed at 900 °C, indicating that the final formation of the Y123 phase is dependent on both the higher final temperature (920 °C) and a longer hold time than was used in the temperature study. By holding the samples at 920 °C for two hours, the quantity of these small impurity phases were reduced (Figure S2).

SQUID magnetometry of the templated Y123 was performed to determine the transition temperature, T_c (Figure 4) and critical current density, J_c (Figure S3, Supporting Information) of the templated Y123. Transition temperatures of 90 ± 1 K and 89 ± 1 K were measured for the foam and paper morphologies, respectively, close to the optimum value for T_c in Y123. The critical current densities were determined at 1 T applied field and 10 K. Values were measured to be 0.10 MA cm^{-2} (foam) and 0.05 MA cm^{-1} (layered).

These values are greater than previously reported values of J_c for commercially available polycrystalline Y123, which are of the order 0.02 MA cm^{-2}.[21] Whilst the values obtained are lower than those known for industrial Y123[35] we believe the templated synthesis technique presented here has the advantage of allowing customization of the morphology of quaternary metal oxides such as YBCO to suit specific applications, while maintaining a good material quality.

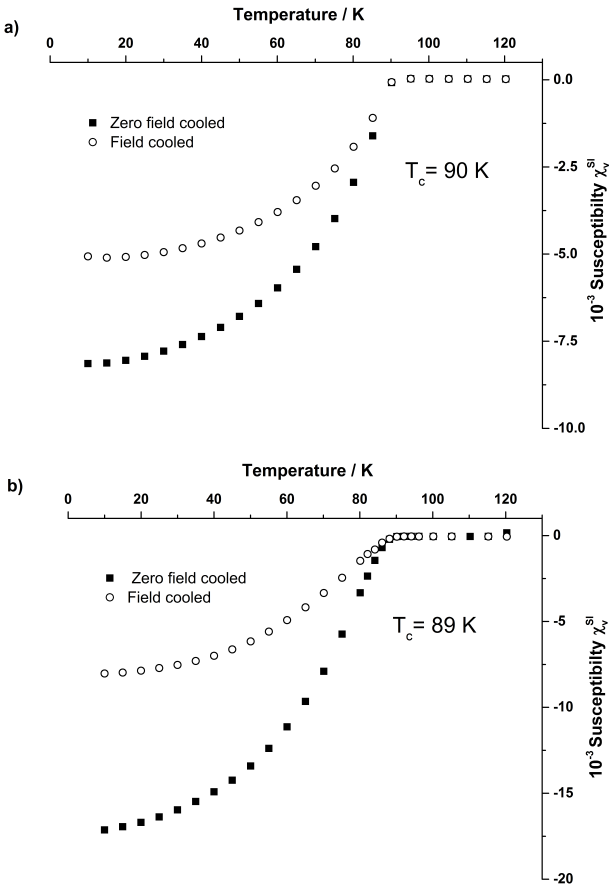

Figure 4. SQUID magnetometry showing superconducting transition temperature, T_c, of a) Y123 foam and b) paper Y123.

In conclusion, we have successfully exploited a novel and highly modifiable template for the construction of materials with pre-determined micro-scale structure, illustrated by the creation of superconducting monoliths with controllable macro- and micro-morphology. We have shown that, due to low temperature stable intermediate phase formation, the final product retains the structure of the uncalcined GO template, allowing porous foams and highly layered superconducting structures to be created. With many further GO morphologies available, this template has potential for great utility in obtaining application-specific morphologies, e.g. foams for rapid access of cryogens to improve cool-down times in superconductors, which retain the desired properties. We have also elucidated the crystallochemical mechanism by which template allows formation of the Y123 phase. This work demonstrates that GO deserves a place alongside biotemplates in the arsenal of options available for creating highly ordered functional inorganic materials.

ASSOCIATED CONTENT

Supporting Information. Experimental information, additional TEM, EDX, XRD and SQUID data. This material is available free of charge via the Internet at http://pubs.acs.org.

AUTHOR INFORMATION

Corresponding Author

*E-mail: simon.hall@bristol.ac.uk

Present Addresses

†R. Boston, Functional Materials and Devices, Materials Science and Engineering, Sir Robert Hadfield Building, University of Sheffield, Mappin Street, Sheffield, S1 3JD.

Author Contributions

‡These authors contributed equally.

Funding Sources

AB, RB and SRH acknowledge the Engineering and Physical Sciences Research Council (EPSRC), UK (grant EP/G036780/1), and RB and SRH the Bristol Centre for Functional Nanomaterials for project funding. VPT thanks the University of Bath for funding via a Prize Fellowship. CFJF thanks the University of Bristol for support.

Notes

The authors declare no competing financial interest

ACKNOWLEDGMENT

All authors would like to acknowledge the Electron and Scanning Probe Microscopy Facility at the School of Chemistry, University of Bristol.

REFERENCES

(1) Tomczak, M. M.; Gupta, M. K.; Drummy, L. F.; Rozenzhak, S. M.; Naik, R. R. *Acta Biomater.* **2009**, *5*, 876–882.

(2) Meldrum, F. C.; Ludwigs, S. *Macromol. Biosci.* **2007**, *7*, 152–162.

(3) Schnepp, Z.; Mitchells, J.; Mann, S.; Hall, S. R. *Chem. Commun.* **2010**, *46*, 4887–4889.

(4) Dong, D.; Wu, Y.; Zhang, X.; Yao, J.; Huang, Y.; Li, D.; Li, C.-Z.; Wang, H. *J. Mater. Chem.* **2011**, *21*, 1028–1032.

(5) Iwahori, K.; Enomoto, T.; Furusho, H.; Miura, A.; Nishio, K.; Mishima, Y.; Yamashita, I. *Chem. Mater.* **2007**, *19*, 3105–3111.

(6) Cung, K.; Han, B. J.; Nguyen, T. D.; Mao, S.; Yeh, Y.-W.; Xu, S.; Naik, R. R.; Poirier, G.; Yao, N.; Purohit, P. K.; McAlpine, M. C. *Nano Lett.* **2013**, *13*, 6197–6202.

(7) Chang, M.-Y.; Wang, W.-H.; Chung, Y.-C. *J. Mater. Chem.* **2011**, *21*, 4966–4970.

(8) Boston, R.; Carrington, A.; Walsh, D.; Hall, S. R. *CrystEngComm* **2013**, *15*, 3763–3766.

(9) Fujikawa, S.; Takaki, R.; Kunitake, T. *Langmuir* **2005**, *21*, 8899–8904.

(10) Boston, R.; Schnepp, Z.; Nemoto, Y.; Sakka, Y.; Hall, S. R. *Science.* **2014**, *344*, 623–626.

(11) Pathak, L. C.; Mishra, S. K. *Supercond. Sci. Technol.* **2005**, *18*, R67–R89.

(12) Wang, H.; Wang, Z.; Huang, L.; Mitra, A.; Holmberg, B.; Yan, Y. *J. Mater. Chem.* **2001**, *11*, 2307–2310.

(13) Smått, J.; Schunk, S.; Linde, M. *Chem. Mater.* **2003**, *15*, 2354–2361.

(14) Banerjee, R.; Furukawa, H.; Britt, D.; Knobler, C.; O'Keeffe, M.; Yaghi, O. M. *J. Am. Chem. Soc.* **2009**, *131*, 3875–3877.

(15) Niwa, M.; Kato, M.; Hattori, T.; Murakami, Y. *J. Phys. Chem.* **1986**, *90*, 6233–6237.

(16) Waterhouse, G. I. N.; Waterland, M. R. *Polyhedron* **2007**, *26*, 356–368.

(17) Kulinowski, K. M.; Jiang, P.; Vaswani, H.; Colvin, V. L. *Adv. Mater.* **2000**, *12*, 833–838.

(18) Culverwell, E.; Wimbush, S. C.; Hall, S. R. *Chem. Commun.* **2008**, *9*, 1055–1057.

(19) Green, D. C.; Lees, M. R.; Hall, S. R. *Chem. Commun.* **2013**, *49*, 2974–2976.

(20) Reddy, E. S.; Noudem, J. G.; Goupil, C. *Energy Convers. Manag.* **2007**, *48*, 1251–1254.

(21) Walsh, D.; Wimbush, S. C.; Hall, S. R. *Chem. Mater.* **2007**, *19*, 647–649.

(22) Lu, Z.; Zhu, J.; Sim, D.; Zhou, W.; Shi, W.; Hng, H. H.; Yan, Q. *Chem. Mater.* **2011**, *23*, 5293–5295.

(23) Lerf, A.; He, H.; Forster, M.; Klinowski, J. *J. Phys. Chem. B.,***1998**, *102*, 4477–4482.

(24) Erickson, K.; Erni, R.; Lee, Z.; Alem, N.; Gannett, W.; Zettl, A. *Adv. Mater.* **2010**, *22*, 4467–4472.

(25) Mi, X.; Huang, G.; Xie, W.; Wang, W.; Liu, Y.; Gao, J. *Carbon N. Y.* **2012**, *50*, 4856–4864.

(26) Qiu, L.; Liu, J. Z.; Chang, S. L. Y.; Wu, Y.; Li, D. *Nat. Commun.* **2012**, *3*, 1241–1248.

(27) Vickery, J. L.; Patil, A. J.; Mann, S. *Adv. Mater.* **2009**, *21*, 2180–2184.

(28) Bai, H.; Li, C.; Wang, X.; Shi, G. *Chem. Commun.* **2010**, *46*, 2376–2378.

(29) Dikin, D. A.; Stankovich, S.; Zimney, E. J.; Piner, R. D.; Dommett, G. H. B.; Evmenenko, G.; Nguyen, S. T.; Ruoff, R. S. *Nature* **2007**, *448*, 457–460.

(30) Cong, H.-P.; Chen, J.-F.; Yu, S.-H. *Chem. Soc. Rev.* **2014**, *43*, 7295–7325.

(31) Dimiev, A. M.; Alemany, L. B.; Tour, J. M. *ACS Nano* **2013**, *7*, 576–588.

(32) Sözeri, H.; Özkan, H.; Ghazanfari, N. *J. Alloys Compd.* **2007**, *428*, 1–7.

(33) Usoskin, A.; Dzick, J.; Issaev, A.; Knoke, J.; Garc, F.; García-Moreno, F.; Sturm, K.; Freyhardt, H. C. *Supercond. Sci. Technol.* **2001**, *14*, 676–679.

(34) Larbalestier, D.; Gurevich, A.; Feldmann, D. M.; Polyanskii, A. *Nature* **2001**, *414*, 368–377.

(35) Schnepp, Z. A. C.; Wimbush, S. C.; Mann, S.; Hall, S. R. *Adv. Mater.* **2008**, *20*, 1782–1786.

SUPPORTING INFORMATION

Experimental section:

Synthesis: Graphene oxide was synthesized *via* the modified Hummers' Method.[1] The GO foam was prepared by a uni-directional freezing method, as reported previously.[2] GO papers were prepared by filtering a GO solution (1 mg mL^{-1}) through an anodisc 0.2μm filter and cutting to the desired size.[1] The resulting monoliths were soaked for 48 h in a stoichiometric aqueous solution of yttrium, barium and copper nitrates (all Sigma Aldrich, UK) in a ratio of 0.05:0.1:0.15 M. The monoliths were then removed from the precursor solution and dried for 12 h at 60 °C, followed by calcination in an alumina boat-shaped crucible at 920 °C for 2 h, with a ramp rate of 10 °C min^{-1}, and cooled to room temperature at a rate of 2 °C min^{-1}. All calcinations were performed in an ELF 11/6 chamber furnace (Carbolite, UK) in air and at atmospheric pressure.

Crystallochemical characterisation: The phases present in the resulting monoliths of YBCO were analysed using powder X-ray diffraction (PXRD) (D8 Advance, Bruker, Germany) using Cu Kα radiation. The macro-scale structure was determined by scanning electron microscopy (SEM) (JSM 6330F, JEOL, Japan). High-resolution transmission electron microscopy (HRTEM) (JEM 2010, JEOL, Japan) was used to image the microscopic crystalline structure of the crystallites and selected area electron diffraction was used to determine the phases of the crystallites observed. Elemental content was determined using energy dispersive X-ray analysis (EDXA) (Oxford Cryosystems, UK) fitted to both the HRTEM and SEM. X-ray μ-computed tomography (NIKON XT H-225ST with a microfocus X-ray source with a 2,000 x 2,000 pixel Perkin Elmer 1620 detector) was used to determine the internal structure of the monoliths, with images produced using Avizo Fire software.

Physical characterisation: Magnetometry was performed using a superconducting interference device (SQUID) (Magnetic Property Measurement System Quantum Design, USA). Samples measured were used as synthesized and placed inside a gelatine capsule. Calculation of J_c was performed using the Bean critical state model.[3] In both cases the crystallite size was found from the measurement of SEM

images, taking the smallest dimension, with the value for the foam being 530 ± 300 nm and for the tape, 460 ± 400 nm.

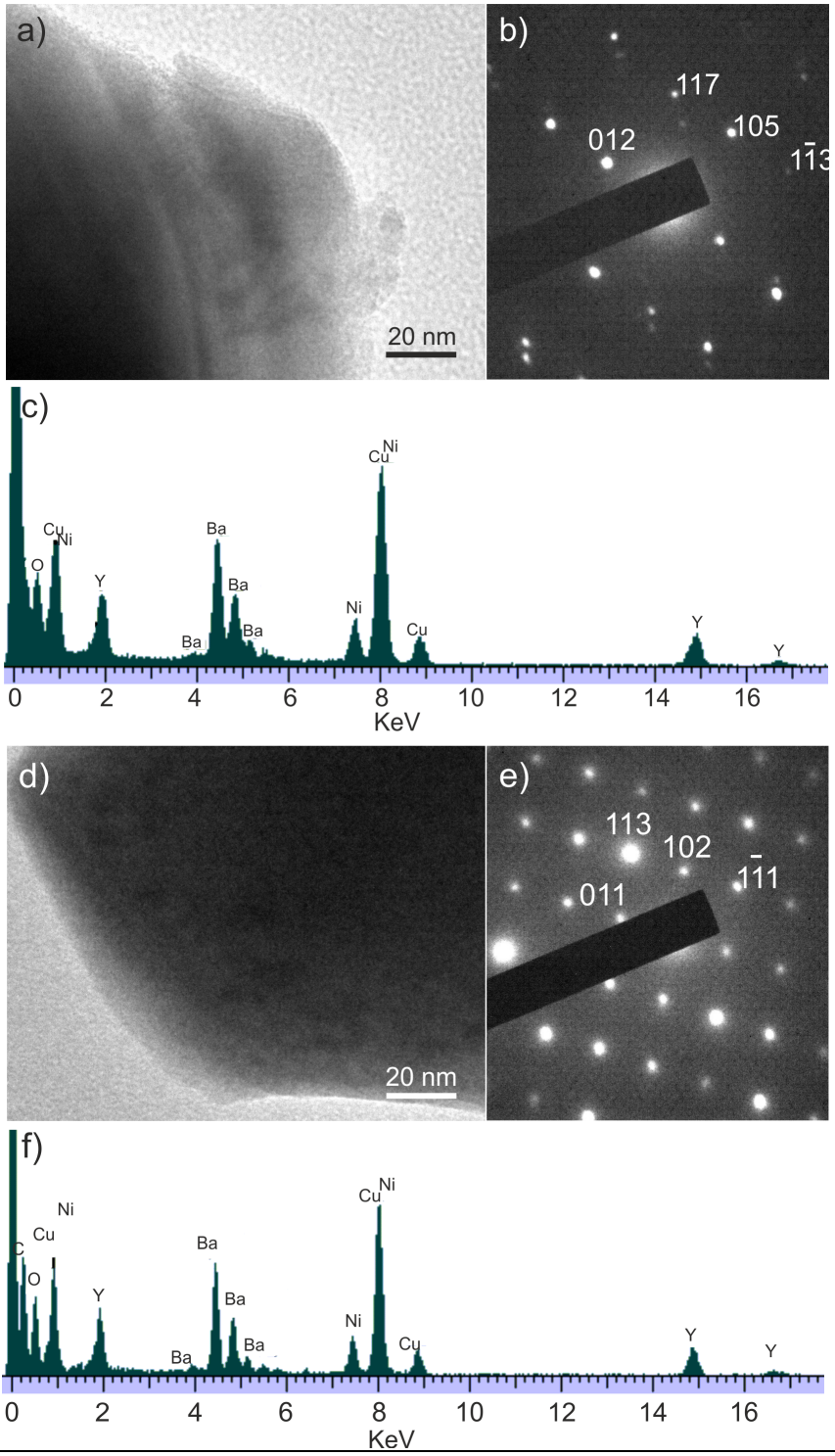

Figure S1. TEM micrographs of crystallites in a) the Y123 foam, with b) corresponding selected area diffraction indexed to the $YBa_2Cu_3O_{6.9}$ phase, and c) corresponding EDXA. d) shows a crystallite of the Y123 tape with e) corresponding selected area diffraction indexed to the $YBa_2Cu_3O_{6.9}$ phase, and f) corresponding EDXA. Nickel is present as the grid material

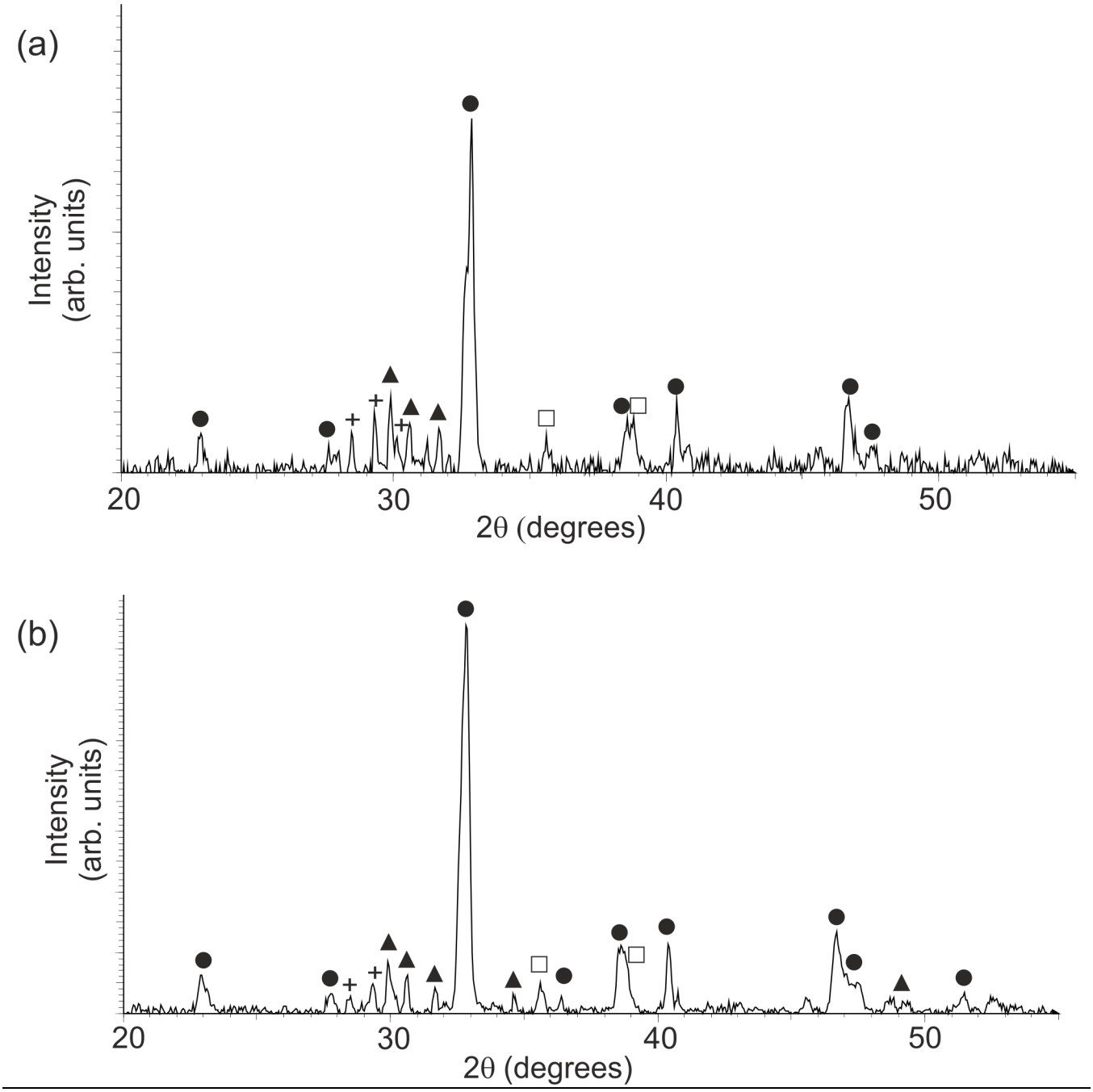

Figure S2: PXRD illustrating the crystalline phases present in a) the Y123 foam and b) the Y123 paper. Phases indexed are $YBa_2Cu_3O_{6.9}$ (●), CuO (□), Y_2BaCuO_5 (▲) and $BaCuO_2$ (+).

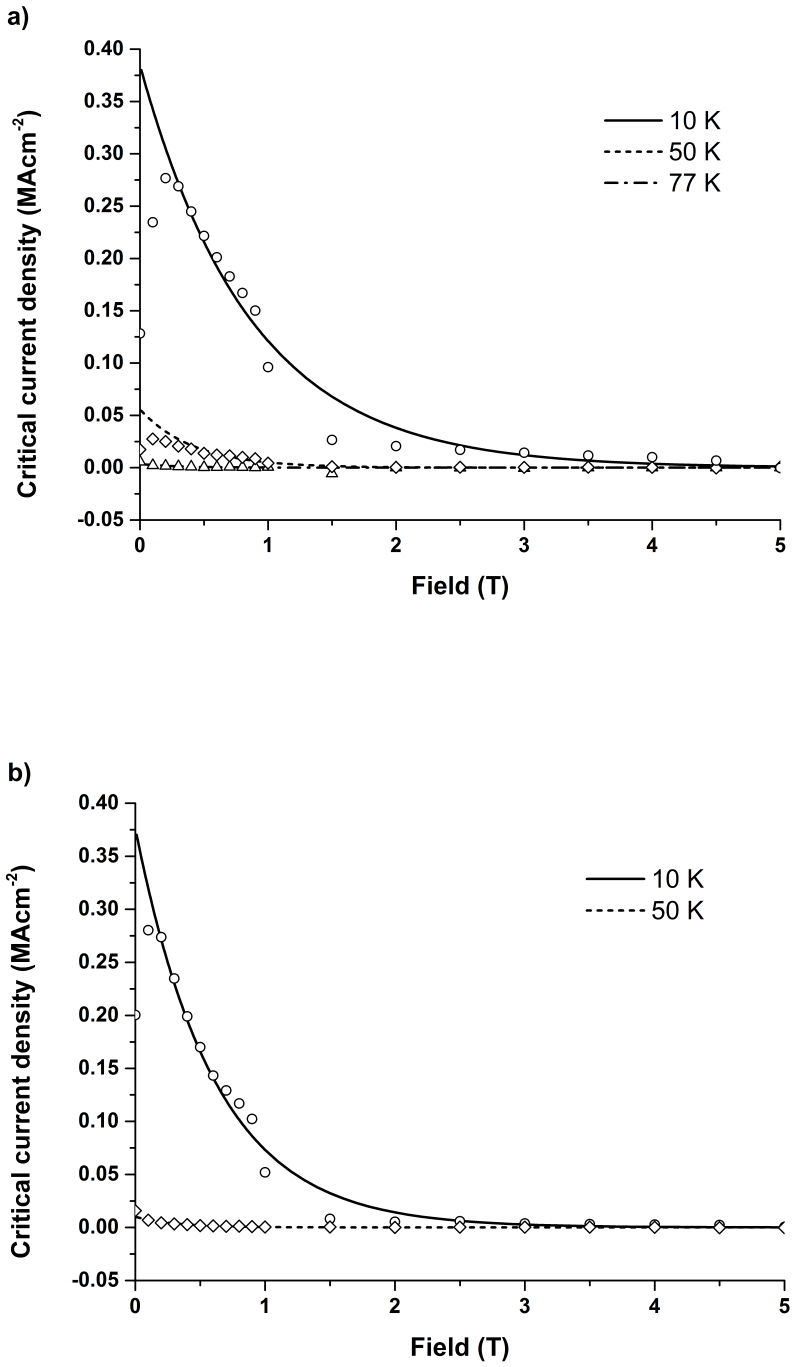

Figure S3. SQUID magnetometry showing critical current density of a) the Y123 foam, and b) the Y123 layered samples. Exponential best fit lines are shown for each dataset.

SUPPORTING INFORMATION REFERENCES

[1] N. I. Kovtyukhova, P. J. Ollivier, B. R. Martin, T. E. Mallouk, S. A. Chizhik, E. V Buzaneva, and A. D. Gorchinskiy, *Chem. Mater.* **1999**, *11* 771–778.

[2] W. L. Li, K. Lu, and J. Y. Walz, *Int. Mater. Rev.* **2012**, *57*, 37–60

[3] P. Bean, *Phys. Rev. Lett.***1962**, *8*, 250253.

Insert Table of Contents artwork here